Electromagnetic Theory of the Loosely Braided Coaxial Cable: Part II—Numerical Results

DAVID A. HILL, SENIOR MEMBER, IEEE, AND JAMES R. WAIT, FELLOW, IEEE

Abstract—**The general modal equation obtained in Part I is solved numerically for the propagation constants of both the monofilar and bifilar modes. For the special case of an air-filled cable, only one mode is supported. Numerical results are also presented for the surface transfer impedance of the shield which, in general, depends on the propagation constant. The properties of the counterwound helical shield are found to be qualitatively similar to those of the unidirectional helical shield.**

I. Introduction

In a previous analysis of a loosely braided coaxial cable [1], an infinite set of linear equations for the shield currents was derived. In this sequel, we utilize the infinite set of equations to obtain numerical results for the propagation constants of the propagating modes of the cable. The properties of these modes are important in utilizing coaxial cables for leaky feeder communications [2].

We also present numerical results for the surface transfer impedance of the cable shield. This quantity has been commonly used to characterize the mean electromagnetic properties of braided cable shields [3], [4], but usually its value has been assumed or measured. Here we calculate the surface transfer impedance in terms of the cable parameters and the propagation constant.

The geometry of the loosely braided coaxial cable is indicated in Fig. 1. The center conductor of radius a is perfectly conducting, and the insulation of permittivity ϵ occupies the region $a<\rho<\rho_0$. The external region, $\rho>\rho_0$, is free space with permittivity ϵ_0, and the entire region external to the center conductor and the shield wires has magnetic permeability μ. The shield consists of Q equally spaced thin-wire helices with pitch angle ψ, and Q counterwound helices with pitch angle $-\psi$. All shield wires have radius c, and a planar development of the shield is illustrated in Fig. 2 for $Q=5$.

Before dealing with the numerical problem, we introduce a modification to the earlier analysis [1] in order to improve numerical convergence. We also obtain approximate analytical expressions for the propagation constant and the surface transfer impedance.

Manuscript received October 19, 1979; revised November 18, 1979.

D. A. Hill is with ITS/NTIA U.S. Department of Commerce, Boulder, CO 80303.

H. J. R. Wait is with ERL/NOAA, U.S. Department of Commerce, Boulder, CO 80303.

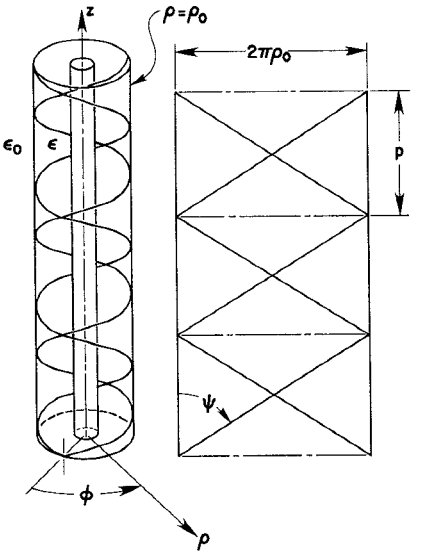

Fig. 1. Perspective view of counterwound helices and planar development of the cylindrical surface (drawn for $Q=1$). The helical wires have radius c.

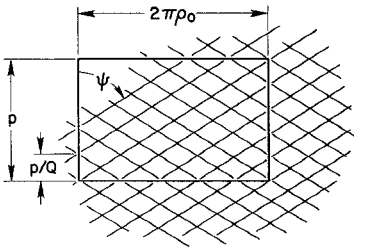

Fig. 2. Planar development of multi counterwound helices (drawn for $Q=5$).

II. Modified Modal Equation

In [1], the series impedance condition (30) that must be satisfied at the helical wires was applied at the top of a wire defined by the spiral, $z=(p/2\pi)\phi+c/\sin\psi$ and $\rho=\rho_0$, where p is the axial period and standard cylindrical coordinates (ρ,ϕ,z) are employed. This resulted in the infinite set of linear equations [1, eq. (49)] for the unknown current coefficients I_m of the helical wires. Since the longitudinal electric field is assumed to be uniform around the circumference of the helical wires, we are actually free to apply the series impedance condition at

any location on the helical wires. For later numerical convenience, we choose the outside of the wire which is defined by the spiral, $z=(p/2\pi)\phi$ and $\rho=\rho_0+c$. Then [1, eq. (49)] becomes

$$\sum_{q=0}^{Q-1}\sum_{n=-\infty}^{\infty} R_{m,n}\exp\left(-i\frac{2\pi nq}{Q}\right)I_m + \sum_{n=-\infty}^{\infty}\hat{R}_{2n+m,n}\exp\left(-i\frac{2\pi nq}{Q}\right)I_{2n+m} + E_z^p\delta_{m,0}\cos\psi = Z_w I_m \quad (1)$$

where E_z^p is the primary field and Z_w is the series impedance of the helical wires. The factor $\exp(-in2\pi c/p\sin\psi)$ in [1, eq. (49)] has been eliminated by applying the impedance condition at $z=(p/2\pi)\phi$. The other change is that ρ_0 in [1, eq. (49)] is replaced by ρ_0+c. Thus, $R_{m,n}$ and $\hat{R}_{m,n}$ are now given by

$$R_{m,n} = -v_{m,n}^2\cos\psi P_{m,n}K_n[v_{m,n}(\rho_0+c)] + i\omega\mu v_{m,n}\sin\psi P_{m,n}^* K_n'[v_{m,n}(\rho_0+c)] + \frac{\sin\psi}{\rho_0+c}n\beta_{m,n}P_{m,n}K_n[v_{m,n}(\rho_0+c)] \quad (2)$$

$$\hat{R}_{m,n} = -v_{m,-n}^2\cos\psi \hat{P}_{m,n}K_n[v_{m,-n}(\rho_0+c)] + i\omega\mu v_{m,-n}\sin\psi \hat{P}_{m,n}^* K_n'[v_{m,-n}(\rho_0+c)] - \frac{\sin\psi}{\rho_0+c}n\beta_{m,-n}\hat{P}_{m,n}K_n[v_{m,-n}(\rho_0+c)] \quad (3)$$

where K_n is a modified Bessel function order n and the remaining quantities are defined in [1].

The form of (1) can be simplified by employing the following identity [1]:

$$\sum_{q=0}^{Q-1}\exp\left(\mp\frac{i2\pi nq}{Q}\right)=\begin{cases} Q, & n=lQ \\ 0, & n\neq lQ\end{cases} \quad (4)$$

where $l=0,\pm1,\pm2,\pm3,\cdots$. Thus, the q summation in (1) can be performed to yield

$$Q\left[\sum_{\substack{l=-\infty\\ n=lQ}}^{\infty} R_{m,n}I_m + \sum_{\substack{l=-\infty\\ n=lQ}}^{\infty}\hat{R}_{2n+m,n}I_{2n+m}\right] + E_z^p\delta_{m,0} = Z_m I_m. \quad (5)$$

To obtain the desired mode equation, we set the primary field E_z^p equal zero and rewrite (5) as

$$\left[\sum_{\substack{l=-\infty\\ n=lQ}}^{\infty} R_{m,n} - \frac{Z_w}{Q}\right]I_m + \sum_{\substack{l=-\infty\\ n=lQ}}^{\infty}\hat{R}_{2n+m,n}I_{2n+m}=0 \quad (6)$$

where (6) holds for $m=0,\pm1,\pm2,\cdots$. From the form of the summations in (6), it is clear that the Fourier coefficients I_m are coupled only for m equal to integer multiples of $2Q$. A convenient finite system of $2P+1$ equations in $2P+1$ unknowns, where P is a positive integer, is then obtained by truncating (6) as follows:

$$\left(S_m - \frac{Z_w}{Q}\right)I_m + \sum_{\substack{l=-P-(m/2Q)\\ n=lQ}}^{P-(m/2Q)} R_{2n+m,n}I_{2n+m}=0 \quad (7)$$

where $S_m = \sum_{l=-\infty, n=lQ}^{\infty} R_{m,n}$ and $m=0, \pm2Q, \pm4Q, \cdots, \pm2PQ$. In the matrix form, (7) is equivalent to

$$\begin{bmatrix}2P+1\\ \text{by}\\ 2P+1\end{bmatrix}\begin{bmatrix} I_{-2PQ}\\ \vdots\\ I_{-2Q}\\ I_0\\ ID_{2Q}\\ \vdots\\ I_{2PQ}\end{bmatrix} = [0]. \quad (8)$$

The homogeneous system of equations in (8) has a nontrivial solution only if the determinant, which is a function of the unknown propagation constant β_0, is zero. Thus, the mode equation is symbolically written

$$\det\begin{bmatrix}2P+1\\ \text{by}\\ 2P+1\end{bmatrix}=0 \quad (9)$$

where the diagonal elements in the square matrix contain the infinite sum S_m. By employing a uniform asymptotic expansion [5] for the Bessel functions in (2), $R_{m,n}$ can be shown to decay exponentially for large n in the manner:

$$R_{m,n}\sim b(n)\exp(-nc\sin\psi\tan\psi/\rho_0) \quad (10)$$

where $b(n)$ is an algebraic function of n. When the match point is taken on the top of the wire, $R_{m,n}$ has only an algebraic decay for large n [1].

III. Approximate Solution

Before proceeding to a numerical solution of (9), it is useful to examine the special case of large Q and perfectly conducting wires (i.e., $Z_w=0$). In view of the exponential decay of $R_{m,n}$ and $\hat{R}_{m,n}$ for larger n, (6) can be written in the following approximate form for $m=0$:

$$(R_{0,0}+\hat{R}_{0,0})I_0=0. \quad (11)$$

From (2), (3), and the previous results in [1], we find that

$$R_{0,0}=\hat{R}_{0,0}. \quad (12)$$

Consequently, the approximate mode equation is

$$R_{0,0}=0. \quad (13)$$

This is identical to the approximate mode equation for the case of unidirectional helices [6]. For $k_0\rho_0$ and $k_0 p$ small, (13) has a solution of the form [6]

$$\frac{\beta_0}{k_0}\simeq\left(\frac{\epsilon}{\epsilon_0}\right)^{1/2}\left[1+\frac{(1-(a^2/\rho_0^2))^{1/2}\tan^2\psi}{2\ln(\rho_0/a)}\right]^{1/2}. \quad (14)$$

For ψ approaching zero, β_0/k_0 approaches $(\epsilon/\epsilon_0)^{1/2}$ and we clearly have the bifilar mode. On increasing ψ, β_0 increases and the mode becomes slower.

Another mode is found numerically for β_0/k_0 slightly greater than unity, but we could find no analytical solution. This mode is clearly the monofilar mode that has the character of an axial surface wave.

IV. Surface Transfer Impedance

The surface transfer impedance Z_T is define as the ratio of the averaged axial electric field at the shield to the averaged axial shield current (proportional to the discontinuity in H_ϕ)

$$Z_T = \frac{\bar{E}_z|_{\rho=\rho_0}}{2\pi\rho_0\left[\bar{H}_\phi|_{\rho=\rho_0^+} - \bar{H}_\phi|_{\rho=\rho_0^-}\right]}. \tag{15}$$

The bar indicates that the averaging is carried out over z (from 0 to p) and ϕ (from 0 to 2π). When this averaging is carried out, only the $m=n=0$ harmonics remain and Z_T is given by

$$\begin{aligned} Z_T = &\left\{E_z^p - 2v_{0,0}^2 A_{0,0} K_0(v_{0,0}\rho_0)\right\} \\ &/\left\{-i\omega 4\pi\rho_0\left\{\epsilon_0 v_{0,0} A_{0,0} K_0'(v_{0,0}\rho_0) - \epsilon_0 \mu B_{0,0}\right.\right. \\ &\cdot\left[I_0'(u_{0,0}\rho_0) - \left[I_0(u_{0,0}a)/K_0(u_{0,0}a)\right]\right. \\ &\left.\left.\cdot K_0'(u_{0,0}\rho_0)\right]\right\}\right\} \end{aligned} \tag{16}$$

where $A_{0,0}$ and $B_{0,0}$ are given in [1].

For the usual case where $u_{0,0}\rho_0$ and $u_{0,0}a$ are small, the small argument approximations for the modified Bessel functions can be used to simplify (16)

$$Z_T \simeq \frac{E_z^p + 2v_{0,0}^2 A_{0,0}\ln(v_{0,0}\rho_0)}{i\omega 4\pi\left[\epsilon_0 A_{0,0} - \epsilon B_{0,0}/\ln(u_{0,0}a)\right]}. \tag{17}$$

For the special case where the mode equation is satisfied, we can set E_z^p equal to zero and (17) further simplifies to

$$Z_T \simeq \frac{v_{0,0}^2 \ln(v_{0,0}\rho_0)}{i\omega 2\pi\left[\epsilon_0 - \epsilon\dfrac{v_{0,0}^2\ln(v_{0,0}\rho_0)}{u_{0,0}^2\ln(\rho_0/a)}\right]}. \tag{18}$$

In order to gain some insight into the dependence of Z_T on pitch angle ψ, we can examine the case for large Q. If the solution for β_0 in (14) is substituted into (18), then Z_T becomes

$$Z_T \simeq \frac{i\omega\mu}{4\pi}\left(1 - \frac{a^2}{\rho_0^2}\right)\tan^2\psi. \tag{19}$$

In many cases the surface transfer impedance is positive and proportional to frequency. This has lead to the following definition [3] for surface transfer inductance L_T:

$$L_T = Z_T/(i\omega). \tag{20}$$

For the special result given by (19), this yields a positive real value of L_T which is independent of frequency. For the more general result of (16), L_T becomes complex and actually depends on both the frequency and the propagation constant.

Another quantity, often quoted for cable shields, is the optical coverage C which is defined as the fraction of metal cover of the shield area. For c small compared with ρ_0 as assumed in [1], it would be given by

$$C = \frac{Qc}{\pi\rho_0\cos\psi}\left(2 - \frac{Qc}{\pi\rho_0\cos\psi}\right) \simeq \frac{2Qc}{\pi\rho_0\cos\psi}. \tag{21}$$

From (21) we see that as ψ increases, the optical coverage increases. However, from (19) or from the numerical evaluation of (16), we find that the cable becomes more leaky (larger $|Z_T|$) as ψ increases. This points up the fact that optical coverage is not a good measure of cable shielding for most cables [7].

V. Numerical Results

A computer program was written to solve the modal equation (9) for the case of perfectly conducting helical wires ($Z_w = 0$). Since the structure is lossless for $Z_w = 0$ and ϵ real, we are interested in real values of β_0 greater than k_0 such that the fields decay for large ρ. The bisection method [8] was used to solve (9), and the truncation effect was examined by increasing P until the value of β_0 converged. In most cases this occurred for $P=2$, and thus a 5 by 5 matrix was sufficient. The surface transfer impedance Z_t was calculated using the general expression (16).

Except where indicated, the following parameters were used: $a = 1.5$ mm, $\rho_0 = 10$ mm, and $c = 0.5$ mm. In all cases μ was taken equal to the free space permeability μ_0. In Figs. 3–6, we show results for the special case $\epsilon = \epsilon_0$, and here only one mode was found.

In Fig. 3, the propagation constant β_0 is shown for various values of Q as a function of pitch angle ψ for a frequency of 10 MHz. As expected, β_0 approaches k_0 for small ψ, and β_0 decreases as the number of shield wires Q increases. The dashed curve for large Q is obtained from (14). In Fig. 4, the surface transfer inductance, $L_T = Z_T/(i\omega)$ (in nanohenrys/meter), is also shown as a function of ψ.

The frequency dependence of the propagation constant is shown in Fig. 5 for $\psi = 30°$. For sufficiently low frequencies, β_0/k_0 is essentially independent of frequency as predicted by the approximate result in (14), but this idealization gradually fails as the frequency is increased. Some frequency dependence also exists for L_T in Fig. 6, but it is less pronounced than in the case of the unidirectional helical shield [6]. Also shown in Figs. 5 and 6 is the result for the assumption of a constant current ($P=0$) on the shield wires. This assumption which was adopted in an earlier analysis by Casey [9] is seen to introduce a small error.

In Figs. 7–10, results are shown for the case of a dielectric insulation, $\epsilon/\epsilon_0 = 2.5$. The propagation constant of the bifilar mode is shown in Fig. 7, and $\beta_0 \simeq k$ for small ψ and large Q as expected. The propagation constant of the monofilar mode is shown in Fig. 8, and β_0 approaches k_0 for small ψ and large Q.

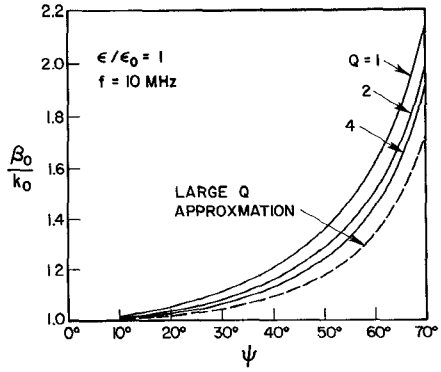

Fig. 3. Relative propagation constant β_0/k_0 as a function of pitch angle for an air-filled cable at a frequency of 10 MHz.

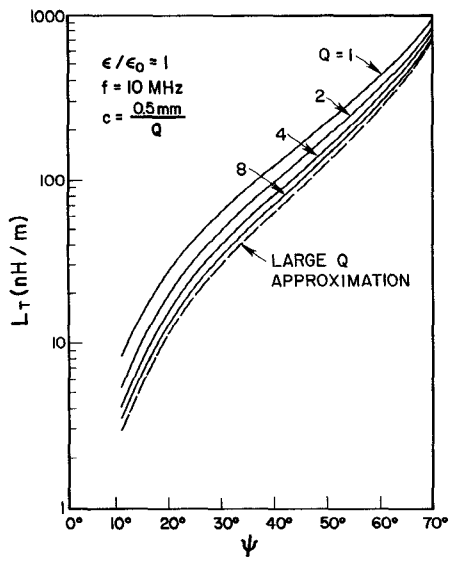

Fig. 4. Surface transfer inductance as a function of pitch angle.

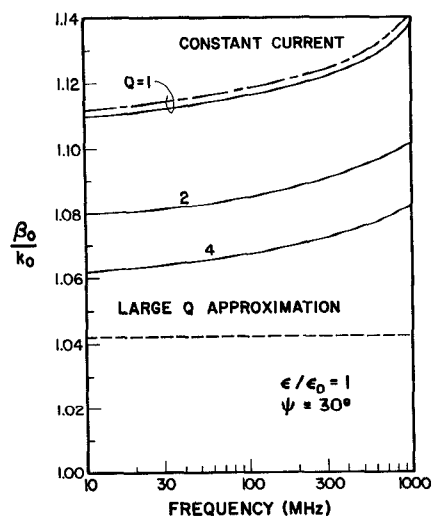

Fig. 5. Relative propagation constant as a function of frequency for an air-filled cable.

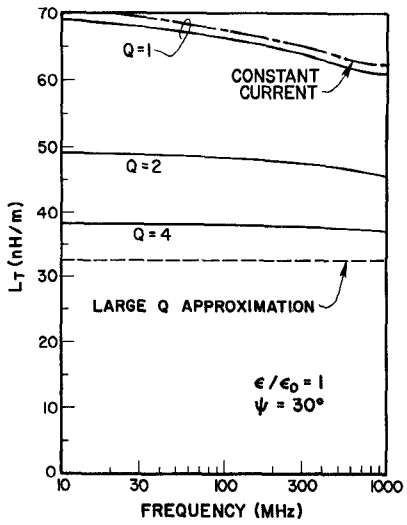

Fig. 6. Surface transfer inductance as a function of frequency.

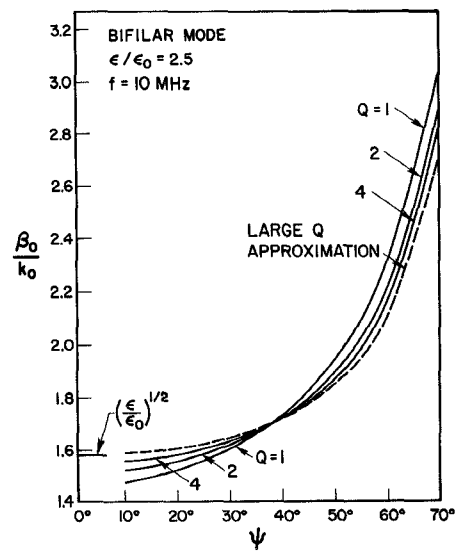

Fig. 7. Relative propagation constant of the bifilar mode of a dielectric-filled cable as a function of pitch angle.

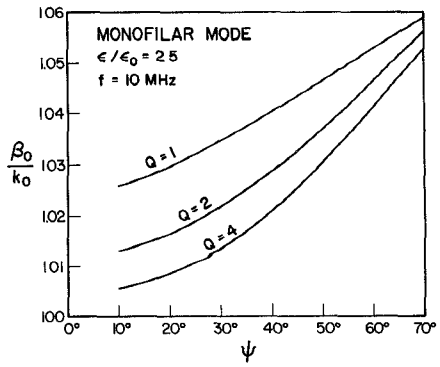

Fig. 8. Relative propagation constant of the monofilar mode of a dielectric-filled cable as a function of pitch angle.

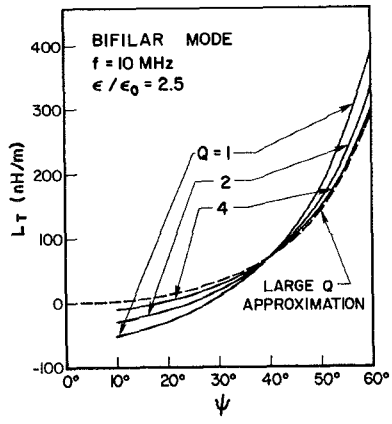

Fig. 9. Surface transfer inductance of the bifilar mode as a function of pitch angle.

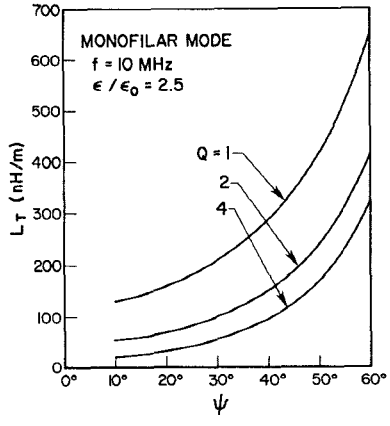

Fig. 10. Surface transfer inductance of the monofilar mode as a function of pitch angle.

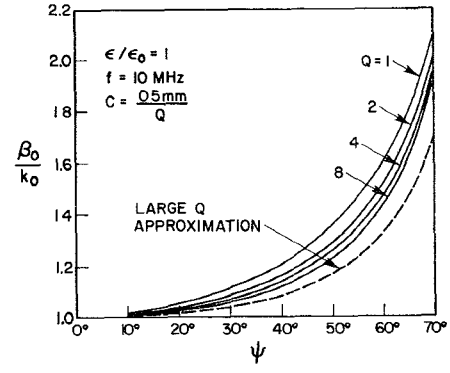

Fig. 11. Relative propagation constant as a function of pitch angle for an air-filled cable. Wire radius c is made inversely proportional to Q for a constant optical coverage.

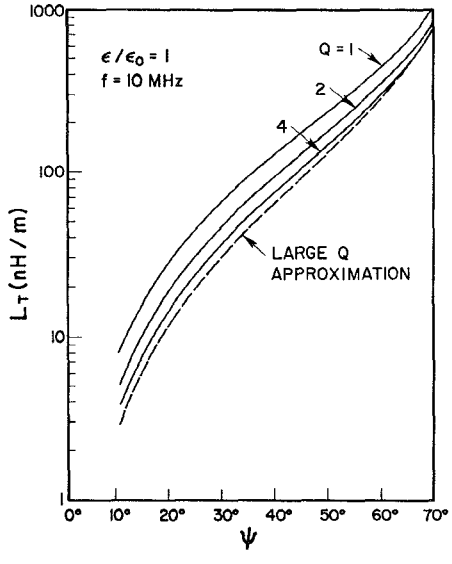

Fig. 12. Surface transfer inductance as a function of pitch angle. Wire radius c is made inversely proportional to Q for a constant optical coverage.

The surface transfer inductance for the bifilar mode is shown in Fig. 9. Since it actually becomes negative for some values of ψ, an inductive reactance is not always an adequate representation for the transfer impedance. The surface transfer impedance for the monofilar mode as shown in Fig. 10 is substantially different from that of the bifilar mode in Fig. 9. Such differences are to be expected since Z_T is known to depend on the propagation constant [10], [11].

In Figs. 11 and 12, the radius c of the helical wires is made inversely proportional to the number of wires Q such that the optical coverage is roughly equal for each Q value. It is seen that β_0 and L_T still decrease as Q is increased, but not as rapidly as in Figs. 3 and 4 where c is held constant. The conclusion is that a large number of thin wires provides better shielding than a small number of thick wires even though the optical coverage is the same.

VI. Concluding Remarks

The modal equation for the propagation constant has been solved analytically for large Q and numerically for the general case. The propagation constant of the bifilar mode is close to the wave number of the insulation. On the other hand, the propagation constant of the monofilar mode is slightly greater than that of free space and it has the character of a Goubau wave. Since there is no return current path for the isolated cable in free space, the monofilar mode takes on the character of a Goubau mode. For the special case of an air-filled cable, only one propagation mode is found.

The surface transfer inductance has been calculated and is generally found to increase with increasing pitch angle. The surface transfer impedance is different for the bifilar and monofilar modes and depends in general on the propagation constant. Optical coverage is found to be a poor indicator of shielding, and a large number of thin wires provides better shielding than a smaller number of thicker wires.

The above conclusions are qualitatively similar to those for the unidirectional helical shield [6]. The primary effect of the counterwound helices is to increase the cable shield-

ing. This generally results in smaller values of both the propagation constant and the surface transfer inductance.

References

[1] J. R. Wait, "Electromagnetic theory of the loosely braided coaxial cable, Part I," *IEEE Trans. Microwave Theory Tech.*, vol. MTT-24, pp. 547–554, Sept. 1976.

[2] J. R. Wait and D. A. Hill, "Propagation along a braided coaxial cable in a circular tunnel," *IEEE Trans. Microwave Theory Tech.*, vol. MTT-23, pp. 401–405, May 1975.

[3] J. Fontaine, B. DeMoulin, P. Degauque, and K. Gabillard, "Feasibility of radio communication in mine galleries by means of a coaxial cable having a high coupling impedance," in *1973 Proc. Thru-the-Earth Electromagnetics Workshop (Colorado School of Mines)*, U. S. Bureau of Mines Contract G-133023, Final Rep., Dec. 31, 1973, pp. 130–139 (available from NTIS, Springfield, VA).

[4] P. Delogne and M. Safak, "Electromagnetic theory of the leaky coaxial cable," *Radio Electron. Eng.*, vol. 45, pp. 233–240, 1975.

[5] M. Abramowitz and I. A. Stegun, Eds., *Handbook of Mathematical Functions.*/ Washington, DC: National Bureau of Standards, AMS-55, 1964, p. 378.

[6] D. A. Hill and J. R. Wait, "Propagation along a coaxial cable with a helical shield," *IEEE Trans. Microwave Theory Tech.*, to be published.

[7] R. J. Slaughter, "Field leakage and crosstalk, with special references to radiating cables with perforated tape screens," *Radio Electron. Eng.*, vol. 45, pp. 248–252, 1975.

[8] R. W. Hamming, *Numerical Methods for Scientists and Engineers*. New York: McGraw-Hill, 1973, pp. 62–63.

[9] K. F. Casey, "Effects of braid resistance and weatherproofing jackets on coaxial cable shielding," Kansas State Univ., Manhattan, Report on Contract AFWL-TR-208 on DNA Subtask EB088; also, Interaction Note 192.

[10] ——, "On the effective transfer impedance of thin coaxial cable shields," *IEEE Trans. Electromagn. Compat.*, vol. EMC-18, pp. 110–116, May 1976.

[11] J. R. Wait and D. A. Hill, "Influence of spatial dispersion of the shield transfer impedance of a braided coaxial cable," *IEEE Trans. Microwave Theory Tech.*, vol. MTT-25, pp. 72–74, Jan. 1977.

Improved Single and Multiaperature Waveguide Coupling Theory, Including Explanation of Mutual Interactions

RALPH LEVY, FELLOW, IEEE

Abstract—**Bethe's small aperture coupling theory, modified by Cohn for large coupling apertures, is improved by including correction terms obtained by averaging the fields over the large aperture. Additionally, inclusion of nonempirical thickness correction factors derived previously by McDonald give coupling formulas which result in theoretical predictions for multiaperture couplers substantially in exact agreement with experiment (correcting small discrepancies previously noted by the author in a 1968 paper). This agreement is now so close that it becomes possible both to identify and explain the mutual interaction effects between closely spaced apertures in multiaperture couplers. It is shown that the mutual interaction is due to contradirectional (or backward) waves in the secondary arm, so that multiaperture interactions are manifested as elimination of the self-interactions of the individual apertures (since the high directivity of typical multiaperture couplers implies negligible backward wave amplitude).**

I. Introduction

THE THEORY OF microwave coupling by large apertures has developed in a number of stages, originating in Bethe's small aperture coupling theory of 1943 [1], [2]. A major extension of Bethe's work has been described by Cohn in 1952 [3], and enabled the theory to be applied to large apertures of finite thickness. Cohn recognized that a coupling aperture between two waveguides has an equivalent circuit representation involving lossless impedances, which must therefore obey Foster's reactance theorem. Hence to take account of the aperture resonance, the impedance was modified simply by inclusion of a factor $(1-f^2/f_0^2)$, where f is frequency and f_0 the resonant frequency of the aperture. The effect of finite thickness was taken into account by treating the aperture as a finite length of waveguide beyond cutoff. However it was noted that this thickness correction was somewhat empirical, and "effective thickness" factors had to be included to give reasonable agreement between theory and experiment.

The Bethe–Cohn theory was applied to the analysis and synthesis of multiaperture waveguide directional couplers by the author in 1968 [4]. It was shown to give excellent results for predicting the directivity of multiaperture couplers, and the coupling could be predicted to within 0.3 dB over most of a complete waveguide band. On the other hand, at high frequencies, between f/f_c values of 1.6 and 1.8, the discrepancy in coupling increased gradually from (typically) 0.3 dB to 0.7 dB, independently of the absolute

Manuscript received June 1, 1979, revised November 2, 1979. This paper was presented at the 1979 IEEE MTT-S Symposium, May 2, 1979, Orlando, FL.

The author is with Microwave Development Laboratories, Inc., Natick, MA 01760.

0018-9480/80/0400-0331$00.75 ©1980 IEEE